
Improving Compositionality of Neural Networks by Decoding Representations to Inputs

Mike Wu, Noah Goodman, Stefano Ermon
Department of Computer Science
Stanford University
Stanford, CA 94303
{wumike,ngoodman,ermon}@stanford.edu

Abstract

In traditional software programs, it is easy to trace program logic from variables back to input, apply assertion statements to block erroneous behavior, and compose programs together. Although deep learning programs have demonstrated strong performance on novel applications, they sacrifice many of the functionalities of traditional software programs. With this as motivation, we take a modest first step towards improving deep learning programs by jointly training a generative model to constrain neural network activations to “decode” back to inputs. We call this design a Decodable Neural Network, or DecNN. Doing so enables a form of compositionality in neural networks, where one can recursively compose DecNN with itself to create an ensemble-like model with uncertainty. In our experiments, we demonstrate applications of this uncertainty to out-of-distribution detection, adversarial example detection, and calibration — while matching standard neural networks in accuracy. We further explore this compositionality by combining DecNN with pretrained models, where we show promising results that neural networks can be regularized from using protected features.

1 Introduction

Traditional hand-written computer programs are comprised of a computational graph of typed variables with associated semantic meaning. This structure enables practitioners to interact with programs in powerful ways (even if they are not the author) — such as debug code by tracing variables back to inputs, apply assertions to block errors, and compose programs together for more complex functionality. However, traditional software has its limitations: it is difficult to hand-write programs to classify images or extract sentiment from natural language. For these functionalities, deep learning and neural networks [41] have become the dominant approach [23, 2, 46].

While neural networks have made impressive progress on complex tasks, they come at a sacrifice of many of the desirable properties of traditional software. Specifically, the closest approximation to a “variable” in a neural network is an activation. Yet it is difficult to understand a neural network’s computation from an activation value, and there is little to associate an activation with semantic meaning. A practitioner cannot write assertion statements to constrain valid neural network logic: checking the values that an activation takes is usually not enough to gauge correctness nor meaning. Moreover, given multiple neural networks, composing them together requires retraining from scratch.

In this paper, we take a modest first step towards bridging the expressivity of deep learning with the engineering practicality of traditional software. We aim to uncover new ways for practitioners to build and use neural networks by leveraging *compositionality*. Specifically, we propose to train a neural network classifier jointly with a generative model whose role is to map the classifier’s activations back to the input, approximating invertibility. For any input, a neural network’s computation can

be represented by a sequence of activations (from each layer), each of which can now be mapped back to the input space. It is this insight that enables a special form of compositionality for neural networks, as inputs derived from activations can be fed back into other models.

In our experiments, we study this compositionality by (1) recursively composing a neural network with itself, creating an ensemble-like model with a measure of uncertainty that is useful for out-of-distribution detection, adversarial example detection, and model calibration; (2) composing neural networks with pretrained models as forms of regularization and distillation; and (3) using decodable activations to discourage a neural network from using protected attributes. Throughout, we show that decodability comes at low cost as we find equivalent accuracy to a standard neural network.

2 Background

Neural Networks We will focus on supervised neural networks for classification, although it is simple to extend to regression tasks. We denote a neural network by f_θ where θ represents its trainable parameters. A neural network f_θ maps an example x to predicted probabilities over K classes. Typically, a neural network is composed of L blocks. For example, if f_θ is a multi-layer perceptron, each block is a linear layer followed by a non-linearity. If f_θ is a ResNet [17], each layer is a residual block. In computing its prediction, a neural network f_θ produces activations $\{h_1, \dots, h_L\}$ where h_l is the output of the l -th block.

To train a neural network, we solve an optimization function of the form

$$\mathcal{L}_{\text{nn}}(x; \theta) = \log p(y|f_\theta(x)) + \beta\Omega(x; \theta) \quad (1)$$

using stochastic gradient descent. In Equation 1, the notation x denotes an input example and y its label. The function Ω represents an auxiliary objective such as a regularizer. The hyperparameter $\beta > 0$ is used to scale the auxiliary loss. For classification, $\log p(y|\cdot)$ is cross entropy.

Generative Models Broadly, we are given a latent variable H and an observed variable X . A generative model g_ϕ captures the distribution $p(x|h)$, mapping samples of the latent code h to samples

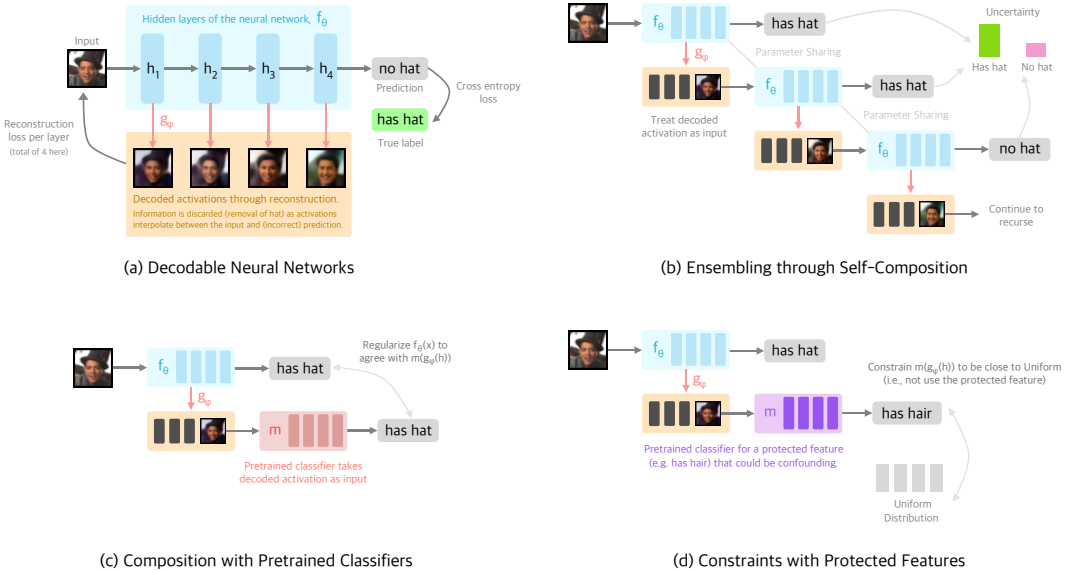


Figure 1: Decodable Neural Networks and Applications: The decodable neural network (DecNN) is composed of a main network, f and a generative model, g . Each activation in f is decoded back to inputs through g . Subfigure (a) shows an incorrect classification: the network predicted the man is not wearing a hat despite the true label. Consequently, we see the decoded activations “interpolate” as the hat is removed. Subfigures (b-d) show the compositionality of DecNNs. First, (b) shows self-composition, where a decoded activation can be fed as input back into the network f to create an ensemble with uncertainty. Second, (c) shows how a pretrained classifier, m can be composed with DecNNs for regularization. Finally, (d) shows how to constrain DecNNs to ignore “protected features” through pretrained networks by regularizing for uniformity.

of the observed variable x . For a deep generative model, g_ϕ is parameterized by a neural network. In the simplest case where g_ϕ is an autoencoder, we are also given an encoder q that maps observed samples x to latent codes h . Then, we optimize the objective

$$\mathcal{L}_{\text{ae}}(x; \phi) = \log p(x|g_\phi(q(x))) \quad (2)$$

where for continuous x , the expression $\log p(x|h)$ is the log Gaussian probability with mean h and fixed variance (or equivalently, mean squared error). More complex generative models might impose a prior distribution on h [22], an adversarial discriminator [29, 14], or invertibility of g_ϕ [35].

3 Neural Networks with Decodable Activations

In Section 1, we motivated our desiderata for activations that can be mapped back to the input space. We now propose to do this by “inverting” a neural network at a particular activation. Concretely, given an input x , a neural network f_θ , we can compute an activation h by computing the forward pass $f_\theta(x)$. Then, suppose we could construct the set:

$$S(h) = \{\hat{x} : \hat{x} \sim p_{\mathcal{D}}, f_\theta(\hat{x}) = h\} \quad (3)$$

where $p_{\mathcal{D}}$ represents the empirical distribution that x is sampled from. Now, any input $\hat{x} \in S(h)$ is a valid mapping of h back to the input space. (Trivially, $x \in S(h)$.) We call this \hat{x} a *decoding* of the activation h . Unfortunately, in practice we do not know how to construct such a set $S(h)$.

But, we do know how to (approximately) sample from $S(h)$. We can train a generative model g_ϕ to reconstruct the original input x from neural network activations h (recall $x \in S(h)$). Then, we can sample $x \sim g_\phi(h)$, which we know how to do, to sample from $S(h)$. If we jointly train this generative model g_ϕ with the neural network f_θ , we can optimize for activations that both solve the classification task and decode back to inputs at once.

So far, we have only considered a single activation despite our neural network having L such activations. Although one could train a separate generative model per layer, we found it efficient and performant to share weights ϕ across all layers. Our joint objective is:

$$\mathcal{L}(x; \theta, \phi) = \log p(y|f_\theta(x)) + \beta \frac{1}{L} \sum_{l=1}^L \log p(x|g_\phi(h_l)), \quad h_1, \dots, h_L \text{ come from } f_\theta(x) \quad (4)$$

where the first term is cross entropy as in Equation 1 and the second term is a reconstruction error (Equation 2) averaged over layers. Comparing Equation 4 to Equation 1, we can interpret the generative loss as a regularization term Ω . Intuitively, in a standard neural network, the activations h_1, \dots, h_L are unconstrained, chosen only to minimize the loss. However, in Equation 4, the network f_θ is constrained to produce activations that the generative model g_ϕ can invert. In practice, g_ϕ is a ResNet-18 decoder with upsampling layers (see Appendix A.1). We call this setup a *Decodable Neural Network*, or DecNN. Figure 1 depicts an illustration of the DecNN architecture.

We highlight that although Equation 4 requires good reconstruction, it does not enforce that reconstructed inputs $f(g_\phi(h))$ must map to the same label y as $f(x)$. We show a few examples of this by visualizing decoded activations throughout a network in Appendix A.3.

4 Composing Decodable Neural Networks

In traditional software, we can easily compose two compatible functions f_1 and f_2 together by $f_2(f_1(x))$ for some input x . With this as loose inspiration, we wish to similarly compose neural networks together. As motivation, we may want to do this to facilitate interaction between networks, such as for regularization or distillation. But given two image classifiers, it is not clear *how to tie outputs from one neural network to inputs for the other?* Both networks expect images as input.

The workaround comes from decodable activations. Since they are images of the same shape as inputs, we are free to treat them as inputs for another model. So, we can compose neural networks together using decoded activations as an intermediary: given two models f_1 and f_2 , and an input x , we can take an activation h coming from $f_1(x)$, decode it, then provide it to the other model, $f_2(g_\phi(h))$. In the following subsections, we explore two instances of this compositionality: one by composing a model with itself (i.e., $f_1 = f_2$), and the other by composing a model f_1 with a pretrained one, f_2 . See Figure 1b,c for a graphical depiction of both compositions.

4.1 Recursive Self-Composition

Our first composition will be to compose a DecNN model with itself. But if we can do that, we can also recursively compose a DecNN model with itself infinitely:

Given a decoded activation $g_\phi(h_l^{(0)})$ for any layer l , we can feed it as input back into the classifier, $f_\theta(g_\phi(h_l^{(0)}))$ and maximize agreement with the true label y . Intuitively, if $g_\phi(h_l)$ is a good reconstruction of the input x (i.e. $g_\phi(h_l)$ and x belong to the same set $S(h_l)$), then a good classifier f_θ should predict the correct label with it as input. Now, we also observe that the computation $f_\theta(g_\phi(h_l^{(0)}))$ produces L additional activations, $h_1^{(1)}, \dots, h_L^{(1)}$ where we use the superscript to represent the number of compositions. We can repeat this exact process with the same intuition, decoding $h_l^{(1)}$ and passing it to f_θ to produce $h_l^{(2)}$. Computational limits aside, this can be repeated ad infinitum.

One interpretation of this procedure is as data augmentation: we saw in Section A.3 that decoded activations share features relevant to the prediction task (e.g. generated celebrities wear hats) but vary other irrelevant features (e.g. face shape, hair color, etc.). Notably, these generated images are not in the original dataset. Thus, training a model using decoded activations as inputs is similar to augmenting the initial dataset. The only difference is that gradients are propagated back through recursion to the inputs, which is also a form of regularization.

Admittedly, what we have described so far is intractable. Besides recursing infinitely, each activation produces L more activations, creating a tree (with root node x) with a large branching factor L . In practice, we make two adjustments — First, we limit the recursion to a max depth D . Second, instead of constructing the full graph of activations, which would have $O(L^D)$ nodes, we randomly sample “paths” in the graph. Specifically, starting at the root, we compute $\{h_1^{(0)}, \dots, h_L^{(0)}\}$ through $f_\theta(x)$ and randomly choose an integer $l_0 \in [1, L]$. Then, we compute $\{h_1^{(1)}, \dots, h_L^{(1)}\}$ through $f_\theta(g_\phi(h_{l_0}^{(0)}))$ i.e. we classify the l_0 -th decoded activation from depth 0. Again, we randomly pick l_1 to compute $\{h_1^{(2)}, \dots, h_L^{(2)}\}$ through $f_\theta(g_\phi(h_{l_1}^{(1)}))$ and repeat until depth D .

Building on Equation 4, we can write this “recursive” objective as:

$$\hat{\mathcal{L}}(x; \theta, \phi) = \log p(y|f_\theta(x)) + \sum_{d=1}^D \alpha^d \log p(y|f_\theta(g_\phi(h_{l_{d-1}}^{(d-1)}))) + \beta \sum_{d=1}^D \alpha^d \log p(x|g_\phi(h_{l_{d-1}}^{(d-1)})) \quad (5)$$

where the sequence of integers l_0, \dots, l_{D-1} are each sampled uniformly from $[1, L]$. We introduce a new hyperparameter $\alpha \in [0, 1]$ that geometrically downweights later depths (if $\alpha = 0$, Equation 5 reduces to maximum likelihood). The first term in Equation 5 is the usual classification objective. The second term is a sum of cross entropy terms that encourage the decoded activation at depth d to predict the correct label through f_θ . The third and final term is a sum of reconstruction losses that encourage the decoded activation at depth d to approximate the original input x .

We call this model a “Recursively Decodable Neural Network”, abbreviated ReDecNN. Note that ReDecNN is a special case of an ensemble network. That is, every path sampled in the activation tree by picking l_0, \dots, l_{D-1} builds a legitimate classifier. There are $O(L^D)$ such classifiers implicit in the ReDecNN. We can interpret optimizing Equation 5 as training individual classifiers that are Monte Carlo sampled from the tree every gradient step. See Figure 1b for an illustration.

Our goal in the next few paragraphs is to utilize this ensemble to measure uncertainty.

Method	MNIST	Fashion	CelebA
Standard	97.1 (0.11)	87.7 (0.19)	90.8 (<0.1)
DecNN	97.8 (0.17)	88.8 (0.19)	90.8 (<0.1)
ReDecNN	97.5 (0.20)	88.1 (0.16)	90.8 (0.16)
Dropout	95.9 (0.13)	80.7 (0.24)	88.5 (0.12)
MC-Dropout	91.3 (0.14)	78.6 (0.23)	87.8 (0.19)
BayesNN	96.3 (0.51)	87.0 (0.36)	88.2 (0.22)
Ensemble	97.6 (0.11)	88.4 (0.12)	90.9 (0.11)

(a) Classification performance on test set.

Method	MNIST	Fashion	CelebA
ReDecNN	0.869	0.795	0.692
MC-Dropout	0.878	0.818	0.657
BayesNN	0.537	0.574	0.587
Ensemble	0.531	0.559	0.605

(b) ROC-AUC of separating correctly classified and misclassified examples using Eq. 6 as a score. The stdev. for all entries over 3 runs are <0.01.

Measuring Uncertainty As a first step, we compare ReDecNN to several baselines: a standard neural network, a neural network with dropout, two kinds of Bayesian neural networks — Monte

Carlo dropout [11], abbreviated MC-Dropout, and weight uncertainty [4], abbreviated BayesNN — and a naive ensemble network where we train D copies of the standard neural network with different initializations. For all experiments, see Appendix A.1 and A.2 for training and task details. Table 1a shows accuracies over a held-out test set, averaged over three runs. While we observe lower accuracy from Bayesian NNs, we observe (perhaps surprisingly) equal performance of DecNN and ReDecNN to a standard neural network. Typically, adding uncertainty to neural networks comes at a cost to performance (as is true for other baselines), but this seems to not be the case here.

The next step is to compare the quality of model uncertainty. For the ReDecNN, for a given input x , we measure uncertainty as follows: sample N different classifiers from the activation tree, and make predictions with each classifier on x . The uncertainty is the entropy of the predictions:

$$\text{Uncertainty}(x) = - \sum_{c=1}^K \hat{p}(y=c) \log \hat{p}(y=c) \quad (6)$$

where $\hat{p}(y=c)$ is the empirical probability (e.g. normalized count) of predicting class c out of N classifiers. A higher uncertainty metric would represent more disagreement between classifiers. We can compute the same metric for a naive ensemble, as well as for MC-Dropout (where repeated calls drop different nodes) and BayesNN (by sampling weights from the learned posterior).

We want to test if the model’s uncertainty is *useful*. One way is to correlate the uncertainty with when the model makes prediction errors (we call this “misclassification”). It would be useful if the model was less uncertain on correct predictions and more uncertain on incorrect ones. A practitioner could then use uncertainty to anticipate when a model might make a mistake. Table 1b reports the area under the ROC curve, or ROC-AUC of separating correctly and incorrectly classified examples in the test set (using uncertainty as a score). A higher ROC-AUC, closer to 1, represents a better separation. We find that ReDecNN is competitive with MC-Dropout, even out performing it on CelebA. In Section A.5, we include examples of images with low and high uncertainty.

Out-of-Distribution Detection A second application of uncertainty is detecting out-of-distribution (OOD) inputs. Given an input that is far from the training distribution, a model is likely to make a mistake. Instead, the model should recognize its uncertainty, and refuse to make a prediction. There is a rich literature on detecting OOD inputs using downstream computation on a trained model [18, 25, 24, 52, 19]. Unlike those works, we study OOD detection using uncertainty alone.

	MNIST			FashionMNIST			CelebA		
	ReDecNN	MC	Ensemble	ReDecNN	MC	Ensemble	ReDecNN	MC	Ensemble
Adversarial (FGSM)	0.787	0.817	0.540	0.711	0.760	0.589	-	-	-
OOD (MNIST)	-	-	-	0.793	0.864	0.501	0.647	0.548	0.591
OOD (FashionMNIST)	0.812	0.888	0.534	-	-	-	0.641	0.572	0.599
OOD (CelebA)	0.893	0.943	0.675	0.753	0.793	0.704	-	-	-
Corrupt (Mean)	0.727	0.785	0.566	0.676	0.691	0.606	0.686	0.569	0.632
Corrupt (Stdv)	0.075	0.113	0.087	0.072	0.108	0.106	0.038	0.017	0.016

Table 2: ROC-AUC of predicting which examples are out-of-distribution (OOD). We vary OOD examples to be adversarial, corrupted, or from a different dataset. Standard deviation for all entries are < 0.01 over three runs.

We explore three kinds of OOD examples: (1) adversarial examples crafted for a single classifier using FGSM [15], (2) examples from a different dataset (e.g. train on MNIST and use FashionMNIST as OOD) as done in [25], and (3) corrupted examples by 14 image transformations (e.g. adding pixel noise), borrowed from [31]. See Appendix A.4 for expanded corruption results.

Table 2 reports the ROC-AUC of separating inlier examples taken from the test split of the dataset the models were trained on, and outlier examples. From Table 2, we observe ReDecNN is just under MC-Dropout, but while MC-Dropout achieves these results at the cost of classification accuracy, ReDecNN does not (Table 1a). Furthermore, we find ReDecNN generalizes better to CelebA, a more complex image dataset, where it outperforms MC-Dropout (and other baselines).

Focusing on CelebA, we study a domain-specific OOD challenge by holding out all images with positive annotations for a single attribute as out-of-distribution. Here, inlier and outlier examples are very similar in distribution. We report ROC-AUCs in Table 3 for three held-out attributes (randomly chosen): is the celebrity in the image “wearing a hat”, has “blonde hair”, or “bald”? As this is a more challenging problem (since inlier and outlier examples are from the same dataset versus different datasets), the performance is lower than in Table 2. But while MC-Dropout, BayesNN, and a naive ensemble all perform near chance, ReDecNN is consistently near 0.6.

OOD: Wearing a Hat		OOD: Blond Hair		OOD: Bald	
Method	ROC-AUC	Method	ROC-AUC	Method	ROC-AUC
ReDecDNN	0.604 (<0.01)	ReDecDNN	0.593 (<0.01)	ReDecDNN	0.615 (<0.01)
MC-Dropout	0.519 (<0.01)	MC-Dropout	0.502 (<0.01)	MC-Dropout	0.502 (<0.01)
BayesNN	0.510 (0.01)	BayesNN	0.508 (0.01)	BayesNN	0.508 (<0.01)
Ensemble	0.526 (<0.01)	Ensemble	0.509 (<0.01)	Ensemble	0.503 (<0.01)

Table 3: We hold out a group of CelebA attributes, such as those wearing a hat, when training. We compute the ROC-AUC of labeling the held-out group as OOD (mean and stdev. over 3 runs).

Calibration A third application of uncertainty we explore is calibration of predicted probabilities. Standard neural networks are notoriously over-confident and are incentivized in training to predict with extreme probabilities (e.g. 0.99). A model with useful uncertainty would make predictions with proper probabilities. Although many calibration algorithms exist [33, 16], we want to measure how calibrated each model is out-of-the-box to compare the quality of model uncertainties.

Table 4a reports the expected calibration error, or ECE [32], which approximates the difference in expectation between confidence and accuracy using discrete bins. A lower number (closer to 0) represents a more calibrated model. We observe that while a standard neural network has a relatively high ECE, many of the approaches (dropout, MC-Dropout, BayesNN, and ReDecNN) reduce ECE. On the other hand, naive ensembles increase the calibration error, as they are more prone to overfitting. In two of three datasets, ReDecNN achieves the lowest ECE whereas MC-Dropout achieves the lowest in the third. These results should be viewed in parallel to Table 1a, which measures “sharpness”. Otherwise, we can trivially reduce ECE to zero by ignoring the input.

Method	MNIST	Fashion	CelebA
Standard	1.18 (0.10)	0.56 (0.14)	2.75 (0.13)
ReDecNN	0.33 (0.05)	0.21 (0.03)	1.92 (0.13)
Dropout	0.63 (0.09)	0.48 (0.09)	2.51 (0.13)
MC-Dropout	0.41 (0.06)	0.13 (0.03)	2.99 (0.15)
BayesNN	0.91 (0.20)	0.18 (0.03)	2.41 (0.19)
Ensemble	1.80 (0.12)	0.89 (0.07)	3.12 (0.12)

(a) We compare the expected calibration error (ECE) of ReDecNN to a standard neural network with various regularization and ensembling.

Depth	Acc.	OOD (Fashion)	OOD (CelebA)
2	97.7	0.665	0.752
4	97.6	0.788	0.804
6	97.7	0.805	0.868
8	97.5	0.812	0.893

(b) Effect of recursion depth D on classification accuracy and OOD detection for a ReDecNN model (8-layer MLP) trained on MNIST.

Effect of Depth Finally, we study the effect of depth on the efficacy of ReDecNN. For the experiments above, we chose the recursive depth to be equal to the number of layers in the MLP ($D = L = 8$). In Table 4b, we vary the depth from 2 to 8 (while keeping the number of layers fixed to 8) and study the effect on classification accuracy and OOD detection. We find increasing OOD performance as D increases, although with marginally decreasing gains. Moreover, we observe constant accuracy, matching standard neural networks regardless of the choice of D .

4.2 Composing with Pretrained Models

Apart from self-composition, we can also compose our neural networks with off-the-shelf pretrained models as a form of regularization or distillation. Suppose we have a pretrained model m that maps an input x to a class prediction. We can modify the ReDecNN objective as follows:

$$\tilde{\mathcal{L}}(x; \theta, \phi) = \hat{\mathcal{L}}(x; \theta, \phi) + \sum_{d=1}^D \alpha^d \log p(f_{\theta}(g_{\phi}(h_{l_{d-1}}^{(d-1)})) | m(g_{\phi}(h_{l_{d-1}}^{(d-1)}))) \quad (7)$$

where $\hat{\mathcal{L}}$ is as defined in Equation 5. The additional term acts as a divergence, bringing the classifier’s predictions close to those of the pretrained model. A similar edit can be made to the DecNN. We revisit Section 4 experiments now using two pretrained models — a linear classifier or a ResNet-18 classifier. For each, we optimize Equation 7 and compute performance on OOD detection.

Table 5 compares the results of composing with either (1) a linear model, (2) a residual network, or (3) no composition (None). Using a linear model, we observe a slight drop in test accuracy but an increase across all OOD experiments and calibration. In fact, these new results rival or surpass MC-Dropout from Table 2. Conversely, with ResNet-18, we observe a 1 point increase in test

Method	MNIST			CelebA		
	None	Linear	ResNet	None	Linear	ResNet
Accuracy	97.50 (0.20)	97.17 (0.12)	98.30 (0.24)	90.80 (<0.1)	89.76 (0.11)	91.28 (0.13)
Misclassification	0.869 (<0.01)	0.904 (<0.01)	0.742 (<0.01)	0.692 (<0.01)	0.732 (<0.01)	0.615 (<0.01)
Adversarial	0.787 (<0.01)	0.805 (0.01)	0.729 (<0.01)	-	-	-
OOD (MNIST)	-	-	-	0.647 (<0.01)	0.693 (<0.01)	0.609 (<0.01)
OOD (Fashion)	0.812 (<0.01)	0.845 (<0.01)	0.650 (<0.01)	0.641 (<0.01)	0.673 (<0.01)	0.585 (<0.01)
OOD (CelebA)	0.893 (<0.01)	0.928 (<0.01)	0.862 (<0.01)	-	-	-
Corruption (Mean)	0.727 (<0.01)	0.790 (<0.01)	0.694 (<0.01)	0.686 (<0.01)	0.708 (<0.01)	0.616 (<0.01)
Calibration (ECE)	0.334 (0.05)	0.296 (0.01)	0.385 (0.02)	1.927 (0.13)	1.937 (0.04)	3.002 (0.10)

Table 5: OOD detection using uncertainty for ReDecNN composed with pretrained models.

accuracy but notable drops in OOD and calibration results. These polarizing outcomes show two use cases of pretrained models: using simpler models allow for regularization that trades off accuracy for robustness while more complex models encourage distillation, making the opposing tradeoff.

Method	Eq. 7	Direct Reg.
Accuracy	97.17	96.72
Misclass.	0.904	0.828
Adversarial	0.805	0.707
OOD (Fashion)	0.845	0.699
OOD (CelebA)	0.928	0.782
Corruption (Mean)	0.790	0.667
Calibration (ECE)	0.296	0.280

Table 6: Composition (Eq. 7) versus direct regularization with pretrained models on MNIST.

as well. Intuitively, constraining the model to be similar to what a pretrained model thinks of the reconstruction (which is a dynamic value that varies with model weights) is a stronger learning signal than what the pretrained model thinks of the original input (which is static). In other words, regularizing $f_\theta(g_\phi(h_k))$ to be like $m(x)$ at all layers l is too strict of a constraint.

An open question is how much Equation 7 benefits from regularizing $f_\theta(g_\phi(h))$ to be close to $m(g_\phi(h))$ versus regularizing it to be close to $m(x)$. The former is a pretrained embedding of a reconstruction whereas the latter is of a static input. Table 6 compares the two on MNIST, where we call the latter “direct regularization”. We observe that Equation 7 outperforms direct regularization (other than calibration), often by a large margin. We reason this to be because the input x and the reconstruction $g_\phi(h)$ can be very different, especially in later layers as shown in Appendix A.3. This implies that $m(x)$ and $m(g_\phi(h))$ can be very different

5 Constraining Decodable Computation

A milestone for deep learning would be the ability to specify what information an activation should *not* capture. This is especially important in cases when we have protected attributes that should not be abused in optimizing an objective. While this milestone remains out of grasp, we take a small step towards it by optimizing a neural network to “be indifferent” with respect to a protected attribute through composition with pretrained models.

Suppose we have access to a pretrained classifier m that predicts the assignment for a K -way protected feature. Then, building on Section 4.2, we can optimize our classifier to “ignore” information about the protected feature through m . To do this, we define the objective:

$$\tilde{\mathcal{L}}(x; \theta, \phi) = \hat{\mathcal{L}}(x; \theta, \phi) + \sum_{d=1}^D \alpha^d \log p(m(g_\phi(h_{l_{d-1}}^{(d-1)})) | \frac{1}{K} \mathbf{1}_K) \quad (8)$$

where $\mathbf{1}_K$ is a K -dimensional vector of ones. That is, Equation 8 encourages the decoded activation $g_\phi(h_{l_{d-1}}^{(d-1)})$, when passed through the protected classifier m , to predict chance probabilities i.e. have no information about the protected attribute. A high performing classifier trained in this manner must have solved the prediction task without abusing the protected attribute(s).

To test this, we extract two attributes from CelebA: “beardedness” and “baldness”. Suppose we wish to design a neural network to predict beardedness. If we were to naively do so, there could be a discrepancy in performance between groups of individuals — for example, between bald individuals and individuals with hair, the latter group is more common in the CelebA dataset. Indeed, Table 7 shows a 10 point difference in F1 and a 5 point difference in average precision (AP) in classifying beardedness between the two groups. The second row of Table 7 provides a baseline ReDecNN

Model	F1 (Bald / Not Bald)	AP (Bald / Not Bald)	ECE (Bald / Not Bald)
Standard	0.338/0.438 ($<0.01 / <0.01$)	19.4/23.9 (0.08 / 0.09)	4.76/3.56 (0.10 / 0.06)
ReDecNN (Eq. 4)	0.327/0.484 ($<0.01 / <0.01$)	18.6/22.3 (0.11 / 0.14)	4.74/3.54 (0.08 / 0.07)
ReDecNN (Eq. 8)	0.461/0.501 (0.01 / <0.01)	27.2/28.9 (0.10 / 0.10)	3.80/3.28 (0.12 / 0.09)

Table 7: We use a pretrained model on CelebA that predicts baldness to optimize the activations of a second classifier to ignore baldness when predicting beardedness.

optimized without knowledge of the protected attribute. Unsurprisingly, we find a similar discrepancy between groups, as with a standard neural network. In the third row, we evaluate a ReDecNN that was optimized to ignore the “baldness” attribute using a pretrained classifier for baldness. Critically, we find much more balanced (and higher) F1, AP, and ECE across the two groups.

Method	F1
Standard	0.383
ReDecNN (Eq. 5)	0.371
ReDecNN (Eq. 8)	0.108

Table 8: Quantitatively accessing ability to classify baldness.

One unsatisfying but plausible explanation for Table 7 is that the generative model learned to construct adversarial examples such that the pretrained model m cannot predict the protected feature, but that the protected feature is still being used to make predictions by f . To show this is not the case, we take a trained ReDecNN optimized by Equation 8, freeze its parameters, and fit a small linear head on top of the last hidden layer to predict the protected feature. If the model learned to ignore this feature, it should not be able to perform the task well. Table 8 reports a poor F1 score (0.1) whereas doing the same with a standard neural network or with an unconstrained ReDecNN gets 3 times the F1 score.

6 Generalizing to other Modalities

While we have focused on image classification, the proposed approach is more general and can be extended to other modalities. We apply the same decodable representations to speech, in particular utterance and action recognition. We compare DecNN and ReDecNN to the same baselines, measuring accuracy and uncertainty through similar experiments as we did for images.

Method	Acc	Misclass.	OOD	ECE	Method	Acc	Misclass.	OOD	ECE
Standard	94.5 (0.1)	-	-	-	Standard	42.4 (0.4)	-	-	-
DecNN	93.8 (0.2)	-	-	-	DecNN	41.4 (0.7)	-	-	-
ReDecNN	93.4 (0.2)	0.766	0.705	0.225 (0.1)	ReDecNN	41.2 (0.5)	0.642	0.605	0.523 (0.2)
MC-Dropout	82.1 (0.4)	0.788	0.745	0.429 (0.2)	MC-Dropout	34.5 (0.7)	0.629	0.562	0.515 (0.2)
BayesNN	91.6 (0.7)	0.545	0.518	1.039 (0.4)	BayesNN	40.3 (1.2)	0.523	0.500	0.918 (0.1)
Ensemble	96.3 (0.1)	0.529	0.506	1.103 (0.2)	Ensemble	44.1 (0.1)	0.541	0.522	1.189 (0.5)

(a) AudioMNIST

(b) Fluent Speech Commands

Table 9: Performance on speech classification. If not specified, stdev. is <0.01 over three test runs.

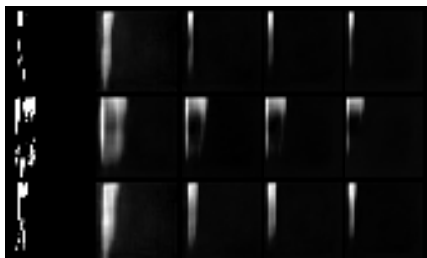


Figure 2: Decoding activations to images for Fluent spectrograms.

We utilize the AudioMNIST [3] and Fluent speech commands [27] datasets, the former being a corpus of 60k utterances of the digits 0 through 9, and the latter a corpus of 100k recordings of 97 speakers interacting with smart-home appliances for one of six actions. Audio waveforms are preprocessed to log Mel spectrograms, outputting a 32 by 32 matrix [47]. Figure 2 shows the input on the left-most column along with the 2nd, 4th, 6th, and 8th decoded activations for 3 random test examples. Table 9 reports the findings, where like the image experiments, we find ReDecNN has strong performance on OOD detection and calibration in return for only a small drop in performance compared to a standard neural network.

7 Related Work

Autoencoders Although DecNNs are reminiscent of autoencoders, there are differences: while autoencoders only reconstruct the final hidden layer, DecNN has a reconstruction for every single hidden layer. This, and because DecNNs have a supervised objective (which autoencoders do not have) critically changes what information is captured in the hidden layers. Whereas the autoencoder seeks perfect reconstruction, the DecNN does not, as evidenced by loss of information for reconstructions later in the network (see Appendix A.3). Finally, we point out that the applications of autoencoders are very different from the DecNN. The former is not used for calibration or composition.

Invertible and Ensemble Networks The DecNN is akin to invertible generative models [6, 36] as DecNN is training a generative model to “invert” the classifier up to a hidden layer. However, unlike invertible flows, DecNN does not impose an explicit prior on the activations (i.e. latent variables), and further, DecNN has a supervised objective. Our proposed recursive network, ReDecNN, has similarities to Bayesian neural networks [11, 4] and ensemble networks [48] — two baselines we compare against for evaluating model uncertainty. However, we find ReDecNN to be easier to train than doing inference over weights, and cheaper in parameter count than naive ensembles.

Probing Neural Networks A related line of work seeks to probe neural network post-training to understand the underlying computation [1]. Most relevant to our work is an approach that inverts CNN activations through reconstruction [28]. Unlike this approach, we are not proposing any additional computation post-hoc. Rather, we are interested in *optimizing* neural networks such that their representations are more easily mapped back to the input domain.

Robustness and Protected Attributes Out-of-distribution detection [26, 24, 52, 40, 20, 19], selective classification [12, 13], adversarial perturbation detection [49, 10, 30, 34], and neural network calibration [16, 51, 50, 32, 38] each have a rich subfield of algorithms. While task-specific methods likely outperform our results, we are excited about representations that enable uncertainty without task information or additional algorithms. Our approach also shares similarities to [42] where the authors minimize the mutual information between learned representations and a protected attribute. We view Equation 8 as an approximation of this where we treat the pretrained classifier for the protected attribute as a proxy for the mutual information.

8 Limitations and Future Work

Method	MNIST	Fashion	CelebA
Standard	13.6 (0.3)	13.5 (0.2)	82.6 (6.2)
DecNN	80.5 (6.8)	99.2 (9.6)	486.2 (12.9)
ReDecNN	96.7 (9.7)	78.6 (6.6)	521.6 (9.2)
Dropout	13.9 (0.6)	14.0 (0.1)	79.5 (5.7)
MC-Dropout	13.9 (0.6)	14.0 (0.1)	79.5 (5.7)
Ensemble	109.6 (7.1)	132.6 (8.5)	659.4 (8.2)

Table 10: Cost (seconds) of 1 epoch on a Titan X GPU (averaged over 10 epochs).

optimizing recursive networks, although parameter efficient, costs more compute as backpropagation is more expensive. See Table 10 for timings of 1 epoch in seconds. The proposed method does have significant computational overhead, averaging about 6x cost, while baseline methods like Dropout and MC-Dropout impose little to no overhead. On the other hand, ReDecNN has comparable cost to DecNN despite requiring recursive gradients. Also, both DecNN and ReDecNN are both cheaper than naive ensembles, significantly in the CelebA case. Future work could explore weight sharing across layers (not just depth) to reduce compute.

In summary, we explored building neural networks with decodable representations, and leveraged this new property to compose models together. By re-purposing decoded activations as novel inputs, we were able to join neural networks together in useful ways for out-of-distribution detection and calibration, as well as influence what information a network retains in optimization. We are optimistic about promising results and look to future research for more applications of decodability.

To close, we discuss a few limitations. First, our approach is bottlenecked by the quality of the generative model. Without a good reconstruction, optimization will be intractable. However, in light recent work [45, 44, 5, 21, 43], this is becoming less of a problem as new generative models surface. Second, in the main text, we only explored feedforward classifiers for simplicity. Our approach extends naturally to residual and transformer blocks, and future research could explore this direction. As a start, we provide experiments for extensions to CNN architectures in Appendix A.6. Third, opti-

Acknowledgments and Disclosure of Funding

We thank the Ermon group for their comments and suggestions. We thank the reviewers for their many iterations of feedback that helped this paper improve significantly. MW is supported by the Stanford Interdisciplinary Graduate Fellowship as the Karr Family Fellow.

References

- [1] Guillaume Alain and Yoshua Bengio. Understanding intermediate layers using linear classifier probes. *arXiv preprint arXiv:1610.01644*, 2016.
- [2] Dzmitry Bahdanau, Kyunghyun Cho, and Yoshua Bengio. Neural machine translation by jointly learning to align and translate. *arXiv preprint arXiv:1409.0473*, 2014.
- [3] Sören Becker, Marcel Ackermann, Sebastian Lapuschkin, Klaus-Robert Müller, and Wojciech Samek. Interpreting and explaining deep neural networks for classification of audio signals. *CoRR*, abs/1807.03418, 2018.
- [4] Charles Blundell, Julien Cornebise, Koray Kavukcuoglu, and Daan Wierstra. Weight uncertainty in neural network. In *International Conference on Machine Learning*, pages 1613–1622. PMLR, 2015.
- [5] Prafulla Dhariwal and Alex Nichol. Diffusion models beat gans on image synthesis. *arXiv preprint arXiv:2105.05233*, 2021.
- [6] Laurent Dinh, Jascha Sohl-Dickstein, and Samy Bengio. Density estimation using real nvp. *arXiv preprint arXiv:1605.08803*, 2016.
- [7] Piero Esposito. Blitz - bayesian layers in torch zoo (a bayesian deep learning library for torch). <https://github.com/piEsposito/blitz-bayesian-deep-learning/>, 2020.
- [8] et al. Falcon, WA. Pytorch lightning. *GitHub. Note: https://github.com/PyTorchLightning/pytorch-lightning*, 3, 2019.
- [9] William Falcon and Kyunghyun Cho. A framework for contrastive self-supervised learning and designing a new approach. *arXiv preprint arXiv:2009.00104*, 2020.
- [10] Reuben Feinman, Ryan R Curtin, Saurabh Shintre, and Andrew B Gardner. Detecting adversarial samples from artifacts. *arXiv preprint arXiv:1703.00410*, 2017.
- [11] Yarín Gal and Zoubin Ghahramani. Dropout as a bayesian approximation: Representing model uncertainty in deep learning. In *international conference on machine learning*, pages 1050–1059. PMLR, 2016.
- [12] Yonatan Geifman and Ran El-Yaniv. Selective classification for deep neural networks. *arXiv preprint arXiv:1705.08500*, 2017.
- [13] Yonatan Geifman and Ran El-Yaniv. Selectivenet: A deep neural network with an integrated reject option. In *International Conference on Machine Learning*, pages 2151–2159. PMLR, 2019.
- [14] Ian J Goodfellow, Jean Pouget-Abadie, Mehdi Mirza, Bing Xu, David Warde-Farley, Sherjil Ozair, Aaron Courville, and Yoshua Bengio. Generative adversarial networks. *arXiv preprint arXiv:1406.2661*, 2014.
- [15] Ian J Goodfellow, Jonathon Shlens, and Christian Szegedy. Explaining and harnessing adversarial examples. *arXiv preprint arXiv:1412.6572*, 2014.
- [16] Chuan Guo, Geoff Pleiss, Yu Sun, and Kilian Q Weinberger. On calibration of modern neural networks. In *International Conference on Machine Learning*, pages 1321–1330. PMLR, 2017.
- [17] Kaiming He, Xiangyu Zhang, Shaoqing Ren, and Jian Sun. Deep residual learning for image recognition. In *Proceedings of the IEEE conference on computer vision and pattern recognition*, pages 770–778, 2016.
- [18] Dan Hendrycks and Kevin Gimpel. A baseline for detecting misclassified and out-of-distribution examples in neural networks. *arXiv preprint arXiv:1610.02136*, 2016.
- [19] Dan Hendrycks, Mantas Mazeika, and Thomas Dietterich. Deep anomaly detection with outlier exposure. *arXiv preprint arXiv:1812.04606*, 2018.

- [20] Dan Hendrycks, Mantas Mazeika, Saurav Kadavath, and Dawn Song. Using self-supervised learning can improve model robustness and uncertainty. In *Advances in Neural Information Processing Systems*, pages 15663–15674, 2019.
- [21] Jonathan Ho, Ajay Jain, and Pieter Abbeel. Denoising diffusion probabilistic models. *arXiv preprint arXiv:2006.11239*, 2020.
- [22] Diederik P Kingma and Max Welling. Auto-encoding variational bayes. *arXiv preprint arXiv:1312.6114*, 2013.
- [23] Alex Krizhevsky, Ilya Sutskever, and Geoffrey E Hinton. Imagenet classification with deep convolutional neural networks. *Advances in neural information processing systems*, 25:1097–1105, 2012.
- [24] Kimin Lee, Kibok Lee, Honglak Lee, and Jinwoo Shin. A simple unified framework for detecting out-of-distribution samples and adversarial attacks. In *Advances in Neural Information Processing Systems*, pages 7167–7177, 2018.
- [25] Shiyu Liang, Yixuan Li, and R Srikant. Enhancing the reliability of out-of-distribution image detection in neural networks. In *International Conference on Learning Representations*, 2018.
- [26] Shiyu Liang, Yixuan Li, and Rayadurgam Srikant. Enhancing the reliability of out-of-distribution image detection in neural networks. *arXiv preprint arXiv:1706.02690*, 2017.
- [27] Loren Lugosch, Mirco Ravanelli, Patrick Ignoto, Vikrant Singh Tomar, and Yoshua Bengio. Speech model pre-training for end-to-end spoken language understanding. *arXiv preprint arXiv:1904.03670*, 2019.
- [28] Aravindh Mahendran and Andrea Vedaldi. Understanding deep image representations by inverting them. In *Proceedings of the IEEE conference on computer vision and pattern recognition*, pages 5188–5196, 2015.
- [29] Alireza Makhzani, Jonathon Shlens, Navdeep Jaitly, Ian Goodfellow, and Brendan Frey. Adversarial autoencoders. *arXiv preprint arXiv:1511.05644*, 2015.
- [30] Jan Hendrik Metzen, Tim Genewein, Volker Fischer, and Bastian Bischoff. On detecting adversarial perturbations. *arXiv preprint arXiv:1702.04267*, 2017.
- [31] Norman Mu and Justin Gilmer. Mnist-c: A robustness benchmark for computer vision. *arXiv preprint arXiv:1906.02337*, 2019.
- [32] Mahdi Pakdaman Naeini, Gregory Cooper, and Milos Hauskrecht. Obtaining well calibrated probabilities using bayesian binning. In *Proceedings of the AAAI Conference on Artificial Intelligence*, volume 29, 2015.
- [33] Alexandru Niculescu-Mizil and Rich Caruana. Predicting good probabilities with supervised learning. In *Proceedings of the 22nd international conference on Machine learning*, pages 625–632, 2005.
- [34] Tianyu Pang, Chao Du, Yinpeng Dong, and Jun Zhu. Towards robust detection of adversarial examples. In *NeurIPS*, 2018.
- [35] George Papamakarios, Eric Nalisnick, Danilo Jimenez Rezende, Shakir Mohamed, and Balaji Lakshminarayanan. Normalizing flows for probabilistic modeling and inference. *arXiv preprint arXiv:1912.02762*, 2019.
- [36] George Papamakarios, Theo Pavlakou, and Iain Murray. Masked autoregressive flow for density estimation. *arXiv preprint arXiv:1705.07057*, 2017.
- [37] Guim Perarnau, Joost Van De Weijer, Bogdan Raducanu, and Jose M Álvarez. Invertible conditional gans for image editing. *arXiv preprint arXiv:1611.06355*, 2016.
- [38] John Platt et al. Probabilistic outputs for support vector machines and comparisons to regularized likelihood methods. *Advances in large margin classifiers*, 10(3):61–74, 1999.
- [39] Robin Rombach, Patrick Esser, and Bjorn Ommer. Network-to-network translation with conditional invertible neural networks. *Advances in Neural Information Processing Systems*, 33, 2020.
- [40] Chandramouli Shama Sastry and Sageev Oore. Detecting out-of-distribution examples with in-distribution examples and gram matrices. *arXiv preprint arXiv:1912.12510*, 2019.

- [41] Jürgen Schmidhuber. Deep learning in neural networks: An overview. *Neural networks*, 61:85–117, 2015.
- [42] Jiaming Song, Pratyusha Kalluri, Aditya Grover, Shengjia Zhao, and Stefano Ermon. Learning controllable fair representations. In *The 22nd International Conference on Artificial Intelligence and Statistics*, pages 2164–2173. PMLR, 2019.
- [43] Jiaming Song, Chenlin Meng, and Stefano Ermon. Denoising diffusion implicit models. *arXiv preprint arXiv:2010.02502*, 2020.
- [44] Yang Song and Stefano Ermon. Generative modeling by estimating gradients of the data distribution. *arXiv preprint arXiv:1907.05600*, 2019.
- [45] Yang Song, Jascha Sohl-Dickstein, Diederik P Kingma, Abhishek Kumar, Stefano Ermon, and Ben Poole. Score-based generative modeling through stochastic differential equations. *arXiv preprint arXiv:2011.13456*, 2020.
- [46] Ilya Sutskever, Oriol Vinyals, and Quoc V Le. Sequence to sequence learning with neural networks. *arXiv preprint arXiv:1409.3215*, 2014.
- [47] Alex Tamkin, Mike Wu, and Noah Goodman. Viewmaker networks: Learning views for unsupervised representation learning. *arXiv preprint arXiv:2010.07432*, 2020.
- [48] Sean Tao. Deep neural network ensembles. In *International Conference on Machine Learning, Optimization, and Data Science*, pages 1–12. Springer, 2019.
- [49] Weilin Xu, David Evans, and Yanjun Qi. Feature squeezing: Detecting adversarial examples in deep neural networks. *arXiv preprint arXiv:1704.01155*, 2017.
- [50] Bianca Zadrozny and Charles Elkan. Obtaining calibrated probability estimates from decision trees and naive bayesian classifiers. In *Icml*, volume 1, pages 609–616. Citeseer, 2001.
- [51] Bianca Zadrozny and Charles Elkan. Transforming classifier scores into accurate multiclass probability estimates. In *Proceedings of the eighth ACM SIGKDD international conference on Knowledge discovery and data mining*, pages 694–699, 2002.
- [52] Ev Zisselman and Aviv Tamar. Deep residual flow for out of distribution detection. In *Proceedings of the IEEE/CVF Conference on Computer Vision and Pattern Recognition*, pages 13994–14003, 2020.

Checklist

1. For all authors...
 - (a) Do the main claims made in the abstract and introduction accurately reflect the paper's contributions and scope? **[Yes]**
 - (b) Did you describe the limitations of your work? **[Yes, please refer to Section 8.]**
 - (c) Did you discuss any potential negative societal impacts of your work? **[Yes, please refer to Section 8.]**
 - (d) Have you read the ethics review guidelines and ensured that your paper conforms to them? **[Yes]**
2. If you are including theoretical results...
 - (a) Did you state the full set of assumptions of all theoretical results? **[No theoretical results]**
 - (b) Did you include complete proofs of all theoretical results? **[No theoretical results]**
3. If you ran experiments...
 - (a) Did you include the code, data, and instructions needed to reproduce the main experimental results (either in the supplemental material or as a URL)? **[Yes, we have included anonymized code in the supplement. All data used is public.]**
 - (b) Did you specify all the training details (e.g., data splits, hyperparameters, how they were chosen)? **[Yes, all choices are specified in detail in the Appendix.]**
 - (c) Did you report error bars (e.g., with respect to the random seed after running experiments multiple times)? **[Yes, please see the tables and captions.]**
 - (d) Did you include the total amount of compute and the type of resources used (e.g., type of GPUs, internal cluster, or cloud provider)? **[Yes, please refer to Appendix.]**
4. If you are using existing assets (e.g., code, data, models) or curating/releasing new assets...
 - (a) If your work uses existing assets, did you cite the creators? **[Yes, for code we borrowed from public implementations, we cite the authors and include URL references in the Appendix.]**
 - (b) Did you mention the license of the assets? **[Yes, please refer to Appendix.]**
 - (c) Did you include any new assets either in the supplemental material or as a URL? **[Yes, we include our source code.]**
 - (d) Did you discuss whether and how consent was obtained from people whose data you're using/curating? **[Not applicable.]**
 - (e) Did you discuss whether the data you are using/curating contains personally identifiable information or offensive content? **[Not applicable.]**
5. If you used crowdsourcing or conducted research with human subjects...
 - (a) Did you include the full text of instructions given to participants and screenshots, if applicable? **[No human subjects experiments]**
 - (b) Did you describe any potential participant risks, with links to Institutional Review Board (IRB) approvals, if applicable? **[No human subjects experiments]**
 - (c) Did you include the estimated hourly wage paid to participants and the total amount spent on participant compensation? **[No human subjects experiments]**

A Appendix

A.1 Training Details

In our experiments, the classifier f_θ is a 8-layer MLP with 128 hidden dimensions per layer. We assume the same dimensionality per layer for simplicity but the approach easily supports MLPs with variable hidden dimensionalities: one can train separate generative models or use the technique from [39] where smaller dimensionalities are padded. The generative model g_θ is a ResNet18 decoder that maps a 128 dimensional vector to a 3 by 32 by 32 pixel image for RGB images and 1 by 32 by 32 for grayscale images and speech spectrograms. We repurpose the implementation from the PyTorch Lightning Bolts [9] repository: https://github.com/PyTorchLightning/lightning-bolts/blob/master/pl_bolts/models/autoencoders/components.py (Apache 2.0 License). (All input images are reshaped to 32 by 32 pixels. No additional image transformations were used in training nor evaluation.) All models are trained for 50 epochs with batch size 128, Adam optimizer with learning rate $1e-4$. We set $\beta = 10$ in all cases. For all ReDecNN models, we use a max depth $D = 8$ and set $\alpha = 0.5$ in all cases. To make for a fair comparison, for all naive ensemble networks, we train 8 copies of a neural network with different weight initializations. For baseline models using dropout and MC-Dropout, we use 0.5 dropout probability. For weight uncertainty (i.e. BayesNN), we use the Blitz library [7], <https://github.com/piEsposito/blitz-bayesian-deep-learning> (GNU V3 License). All pretrained models used were ResNet-18 classifiers. Our ResNet classifier implementation was adapted from `torchvision`. For each of the architectures, to support 32x32 images (which are smaller than the standard), we replace the first 7x7 convolutional layer with a 3x3 convolutional layer and reduce the first max pooling layer. We did not use their pretrained weights from `torchvision` and instead trained them ourselves on MNIST, FashionMNIST, and CelebA from scratch (again 50 epochs). All models were trained on a single Titan Xp GPU with 4 CPUs for data loading. An average model takes 1 hours to train for MNIST and FashionMNIST and 4 hours for CelebA, and speech experiments. In our experiments, we compute uncertainty using 30 random samples (e.g. for ReDecNN, this is 30 paths; for MC-Dropout, this is 30 different dropout configurations, etc.). ROC-AUC computation is done through `scikit-learn` (BSD License). In CelebA, only a subset of 18 attributes are used, chosen for visual distinctiveness as done in [37]. Conveniently, this removes many trivial features that are mostly of a single class as well. In experiments, we utilize the PyTorch Lightning framework [8] (Apache 2.0 License) and Weights and Biases (MIT License) for tracking. For speech experiments, the AudioMNIST dataset is found at <https://github.com/soerenab/AudioMNIST> (MIT License) and the Fluent dataset can be downloaded at <https://fluent.ai/fluent-speech-commands-a-dataset-for-spoken-language-understanding-research/> (academic license). All speech spectrograms are normalized using a mean and standard deviation computed from the training dataset. We use `torchaudio` and `librosa` to efficiently compute Mel spectrograms.

A.2 Dataset & Task Details

We describe the setup for each set of results presented in the main text, paying close attention to the data used, and any special setup required.

Table 1a For classification, we use datasets as in standard practice. MNIST and FashionMNIST are both classification tasks with 10 classes. CelebA has 18 binary attributes, and we optimize an objective containing the sum of 18 binary cross entropy terms, one for each attribute. Accuracy is reported using the respective test set.

Table 1b Given all test examples, we make predictions and get uncertainty scores using the trained model. We split the test set into two groups, those we correctly classified, and those we misclassified. Then, we compute the ROC-AUC with uncertainty as the prediction score. An ROC-AUC of 1 would mean that the model perfectly assigned high uncertainty to examples it misclassified.

Table 2 OOD detection experiments are very similar to the misclassification experiments except we define groups differently. Generally, there is inlier group and an outlier group. We compute uncertainty scores over both groups and then compute ROC-AUC with uncertainty as the prediction score. An ROC-AUC of 1 would mean that the model perfectly assigned high uncertainty to outlier examples. Table 2 has three different ways of defining inliers and outliers. First, fixing a dataset and trained classifier, we can compute adversarial examples with FGSM on the test set. This serves as the

outlier set while the original test set serves as the inlier. Second, for rows labeled OOD (XXX), we take the test set from dataset XXX to be the outlier set while the test set from training dataset acts as the inlier set. Finally, for corruptions, we compute image transformations on the test set (e.g. blur all image in the test set) and treat this as the outlier set (again, the original test set acts as the inlier set). We do this separately for each corruption transformation, and report the average and standard deviation (over corruptions) in the main text.

Table 3 In Table 2, we limited OOD experiments to using a separate dataset as outliers. For CelebA, we can consider a more difficult task by holding out all images with a positive label for a single attribute. We consider three such attributes: hold out all people wearing a hat, all people with blond hair, or all people who are bald. Because a model with uncertainty has not seen any images of people wearing hats (for example), it should assign these images higher uncertainty. The difficulty of this task comes from outlier and inlier inputs being very similar in features; they are now both images of celebrities, rather than images of digits. In all cases, the inlier set is defined to be all test set images without a positive label for the held out attribute.

Table 4a ECE is computed on predicted probabilities using the test set for MNIST, FashionMNIST, and CelebA separately. The labels used for binning are the standard dataset annotations.

Table 4b Same setup as in Table 2 but we vary the recursion depth for ReDecNN.

Table 5 Design of experiments in the Table are as described above for misclassification, OOD, and calibration. We pretrain a linear model and a ResNet-18 model using the training set of MNIST and CelebA, separately. For CelebA, pretrained models optimize a sum of 18 binary cross entropy terms.

Table 6 Same setup as in Table 5.

Table 7 Using the CelebA dataset, we discard all attributes except the “baldness” and “beardedness” columns (note this does not change the size of the dataset). We fit a ResNet-18 model to predict baldness only (here, we do not use the beardedness label). Following this, we train a ReDecNN with Equation 8 to ignore the protected attribute (baldness) when predicting beardedness. We then compute the F1, AP, and ECE scores separately for two groups, one containing images of all bald individuals in the test set and one containing images of all non-bald individuals in the test set. These two groups will not be equal in size but are sufficiently large to compute statistics.

Table 8 Given the CelebA dataset, we only use the “baldness” attribute. Given a trained model (a standard neural network or a ReDecNN), we freeze its parameters, find the last hidden layer (the L -th one), and initialize linear head on top. This linear head returns a binary prediction: bald or not bald. We optimize this model with binary cross entropy and see if the frozen weights contain the information to predict baldness.

Table 9 See Appendix A.1 for the dataset links for AudioMNIST and Fluent Speech Commands. We preprocess waveforms in each to be mel spectrograms of fixed size $1 \times 32 \times 32$, mimicking the CIFAR10 setup (note that there is only 1 channel). See Figure 2 left-most column for three examples of input spectrograms. AudioMNIST has 10 output labels whereas Fluent Speech Commands has 6 output labels. The task and data setup remain the same as in Table 2 for OOD, misclassification, and calibration experiments.

Table 10 Given a dataset and model, we use the `time.time` function in Python to record the start and end times for each epoch on a Titan X GPU. We do so for 10 contiguous epochs and report the average (and standard deviation). Eight data workers are used to load images (increasing this will decrease the cost per epoch).

Table 11 This is identical to Table 2 but does not report the average over corruption experiments, but reports each individually.

Table 12 This is identical to Table 2 but replaces an MLP with stacked convolutional layers.

A.3 Visualizing Decodable Activations

The most straightforward application of decodable activations is that we can visualize them. Figure 3 shows randomly chosen examples taken from DecNNs trained on FashionMNIST and CelebA. In each subfigure, the leftmost column is from the dataset while the remaining eight columns are decoded activations from layer 1 to 8 (f_θ is an MLP with $L = 8$ layers).

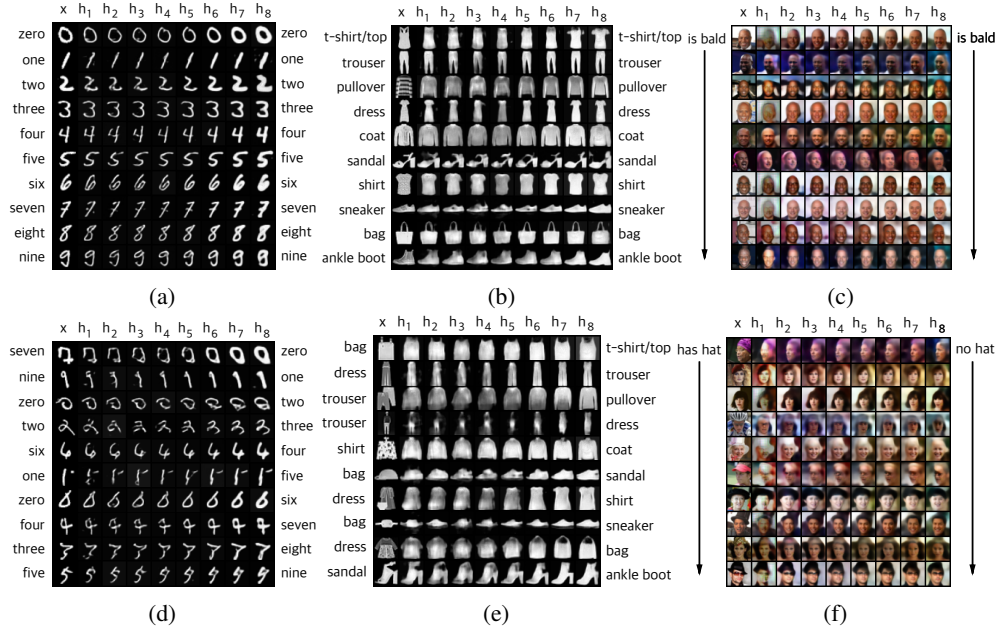


Figure 3: *Visualizing activations*: the top row shows decoded activations when the model correctly classified examples; the bottom row shows misclassifications.

The top row of three subfigures shows decoded activations for correctly-classified examples whereas the bottom row of three subfigures shows mis-classified examples, all randomly chosen. For correctly-classified examples, we observe that the decoded activations tends toward class prototypes. Decoded images from the 7th or 8th activation lose details (e.g. patterns, logos, or shoe straps disappear from clothing). The top row of Figure 3b presents a good example: the tank-top (a rare form of the t-shirt) is projected to a more prototypical t-shirt. Furthermore, we also find that mis-classified examples morph into images of the incorrect class. The seventh row of Figure 3e morphs the two articles of clothing that compose the dress to build a shirt. The seventh row of Figure 3f show the celebrity’s hat transform into a background color.

Although we may be tempted to interpret these activations as revealing what the neural network is learning, the objective (Equation 4) does not guarantee this, as reconstructions could appear visually similar to the input x but map to completely different outputs y , and as such, serve as a poor explanation as to what the underlying function f is doing. Future work could consider also constraining reconstructions to map to the same label as $f(x)$.

A.4 Extended OOD Results

We provide a more thorough breakdown of performance for the 14 different image corruptions. In the main paper, we only show the average performance over all corruptions.

A.5 Visualizing OOD Examples

In the main paper, we present OOD results using ROC-AUC. Here, we visually inspect some examples the model deems as OOD. Figure 4 shows one image from each class (of MNIST, FashionMNIST, and CIFAR10) with low and high uncertainty. We observe that high uncertainty images are less prototypical. For example, the high uncertainty digits in Figure 4d have accented curvature, whereas the high uncertainty clothing in Figure 4e have more atypical designs, and the high uncertainty images of celebrities in Figure 4f, although annotated as not bald, are wearing hats or have thin hairlines and exposed foreheads. On the other hand, low uncertainty images in all datasets look more prototypical.

	MNIST			FashionMNIST			CelebA		
	ReDecNN	MC	Ensemble	ReDecNN	MC	Ensemble	ReDecNN	MC	Ensemble
Adversarial (FGSM)	0.787	0.817	0.540	0.711	0.760	0.589	todo	todo	todo
OOD (MNIST)	-	-	-	0.793	0.864	0.501	0.647	0.548	0.591
OOD (FashionMNIST)	0.812	0.888	0.534	-	-	-	0.641	0.572	0.599
OOD (CelebA)	0.893	0.943	0.675	0.753	0.793	0.704	-	-	-
Corrupt (Brightness)	0.851	0.955	0.702	0.732	0.667	0.816	0.653	0.558	0.623
Corrupt (Dotted Line)	0.672	0.684	0.546	0.602	0.589	0.535	0.647	0.559	0.626
Corrupt (Glass Blur)	0.664	0.718	0.515	0.617	0.584	0.525	0.641	0.596	0.652
Corrupt (Impulse Noise)	0.702	0.848	0.551	0.702	0.746	0.642	0.683	0.555	0.640
Corrupt (Rotate)	0.689	0.714	0.523	0.754	0.839	0.600	0.645	0.585	0.652
Corrupt (Shear)	0.685	0.661	0.502	0.611	0.809	0.543	0.750	0.581	0.636
Corrupt (Spatter)	0.647	0.683	0.502	0.617	0.615	0.534	0.715	0.569	0.641
Corrupt (Translate)	0.809	0.889	0.511	0.725	0.826	0.555	0.673	0.577	0.610
Corrupt (Canny Edges)	0.696	0.824	0.521	0.703	0.807	0.571	0.649	0.569	0.650
Corrupt (Fog)	0.868	0.940	0.732	0.748	0.670	0.810	0.729	0.608	0.643
Corrupt (Scale)	0.768	0.846	0.535	0.808	0.805	0.521	0.750	0.562	0.632
Corrupt (Shot Noise)	0.617	0.559	0.526	0.541	0.537	0.528	0.685	0.542	0.592
Corrupt (Stripe)	0.804	0.892	0.755	0.684	0.522	0.772	0.674	0.563	0.628
Corrupt (Zigzag)	0.709	0.785	0.514	0.626	0.658	0.532	0.714	0.555	0.627
Corrupt (Mean)	0.727	0.785	0.566	0.676	0.691	0.606	0.686	0.569	0.632
Corrupt (Stdev)	0.075	0.113	0.087	0.072	0.108	0.106	0.038	0.017	0.016

Table 11: We report the ROC-AUC of predicting which examples are out-of-distribution (OOD) using uncertainty. We vary OOD examples to be adversarial, corrupted, or taken from a different dataset.

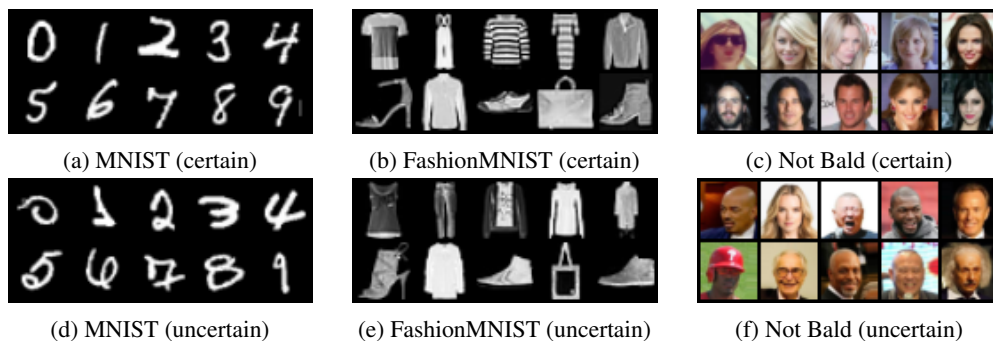


Figure 4: *Randomly sampled images with low and high uncertainty.* Images with high uncertainty appear less “prototypical”. Figure 4(c,h) shows images from CelebA annotated as “not bald”. We observe images that the model is uncertain about depict individuals with a thin hair line, exposed foreheads, or wearing helmets.

A.6 Extensions to CNN Architectures

In the main text, we limited the experiments to MLP architectures for simplicity. Here, we include a subset of the experiments in Section 4, replacing the MLP with stacked convolutional layers.

For this experiment, we use architectures of 8 total convolutional layers with ReLU nonlinearity and 64 filters. We use a U-Net decoder (again with 64 filters) as the generative model, which is better suited to convolutional activations (which are now three dimensional rather than two). Like before, we optimize for 50 epochs, batch size 128, learning rate $1e-4$, and use Adam. For a baseline, we compare against MC-Dropout, the most competitive baseline from the main text.

Method	Acc.	Misclass.	OOD (MNIST)	OOD (CelebA)	Corruption (Mean)	Calibration (ECE)
Standard	90.2	-	-	-	-	1.848
DecNN	90.6	-	-	-	-	-
ReDecNN	89.5	0.876	0.883	0.844	0.712	0.837
MC-Dropout	85.9	0.863	0.776	0.895	0.723	0.889

Table 12: DecNN with convolutional layers trained on FashionMNIST.

From Table 12, we see similar findings to the MLP results, although overall performance is higher due to a more expressive architecture. Namely, ReDecNN, DecNN, and a standard NN have similar test accuracy whereas MC-Dropout has a 4 point lower accuracy. When using the uncertainty score to detect misclassification, OOD, and corruption, we find much closer performance between MC-Dropout and ReDecNN (whereas in the paper, MC-Dropout outperformed ReDecNN on FashionMNIST

consistently), which is promising. Finally, for calibration, MC-Dropout and ReDecNN are again comparable, with the latter having a slightly lower ECE score.